
HOKKAIDO UNIVERSITY

Title	Frequency response function measurements of rotational degrees of freedom using a non-contact moment excitation based on nanosecond laser ablation
Author(s)	Hosoya, Naoki; Ozawa, Shota; Kajiwara, Itsuro
Citation	Journal of sound and vibration, 456, 239-253 https://doi.org/10.1016/j.jsv.2019.05.024
Issue Date	2019-09-15
Doc URL	http://hdl.handle.net/2115/75008
Rights(URL)	http://creativecommons.org/licenses/by-nc-nd/4.0/
Type	article
File Information	1-s2.0-S0022460X19302937-main.pdf


Instructions for use

Hokkaido University Collection of Scholarly and Academic Papers : HUSCAP

Journal of Sound and Vibration 456 (2019) 239–253

Contents lists available at ScienceDirect

Journal of Sound and Vibration

journal homepage: www.elsevier.com/locate/jsvi

Frequency response function measurements of rotational degrees of freedom using a non-contact moment excitation based on nanosecond laser ablation

Naoki Hosoya [a, *], Shota Ozawa [b], Itsuro Kajiwara [c]

[a] Department of Engineering Science and Mechanics, Shibaura Institute of Technology 3-7-5 Toyosu, Koto-ku, Tokyo 135-8548, Japan
[b] Division of Mechanical Engineering, Shibaura Institute of Technology 3-7-5 Toyosu, Koto-ku, Tokyo, 135-8548, Japan
[c] Division of Human Mechanical Systems and Design, Hokkaido University N13, W8, Kita-ku, Sapporo, 060-8628, Japan

ARTICLE INFO

Article history:
Received 17 September 2018
Received in revised form 8 May 2019
Accepted 13 May 2019
Available online 21 May 2019
Handling Editor: H. Ouyang

Keywords:
Frequency response function
Rotational degrees of freedom
Moment excitation
Laser ablation
Non-contact vibration tests

ABSTRACT

Frequency response functions (FRFs) are generally measured by investigating the input–output relationship of a target structure. An input is applied to the target structure and the output is measured. Typical vibration tests measure inputs as excitation forces using load cells or similar devices and outputs as velocities or accelerations using laser Doppler vibrometers or accelerometers. Each input or output has three translational degrees of freedom (DOF). Consequently, experimental models established based on such tests have three translational DOF. However, numerical models using finite element analysis (FEA) for existing structures have six DOF at each node (three translational and three rotational DOF). Therefore, numerical models using FEA and experimental models have gaps in their DOF, leading to diverse problems. This study realizes a non-contact measurement method for rotational DOF FRFs using an impulse excitation force generated by laser ablation (LA) where the input is a moment and the output is the velocity. A laser beam radiated from an Nd:YAG pulse laser emitter is divided using a half mirror, halving the laser pulse energy. Then, these laser beams are radiated on two points near a target structure's excitation point. The simultaneous occurrence of LA at these two points realizes a moment that acts on the target structure in a non-contact manner. This experiment uses a 5052 aluminum alloy plate where one end is fixed as a test piece. Both the auto FRFs and cross FRFs for the rotational DOF between two arbitrary points on the test piece are measured. The FRFs obtained by our method agree well with those obtained by FEA, demonstrating its efficacy.

© 2019 The Authors. Published by Elsevier Ltd. This is an open access article under the CC BY-NC-ND license (http://creativecommons.org/licenses/by-nc-nd/4.0/).

1. Introduction

Various vibration measurement methods that assess frequency response functions (FRFs) have been proposed to determine the dynamic characteristics of structures [1–8]. These methods determine the relationships between applied inputs and measured outputs. Typically, inputs are measured as excitation forces using load cells or similar devices, while outputs are measured as velocities or accelerations using laser Doppler vibrometers (LDVs) or accelerometers.

* Corresponding author.
E-mail addresses: hosoya@sic.shibaura-it.ac.jp (N. Hosoya), md15018@shibaura-it.ac.jp (S. Ozawa), ikajiwara@eng.hokudai.ac.jp (I. Kajiwara).

https://doi.org/10.1016/j.jsv.2019.05.024
0022-460X/© 2019 The Authors. Published by Elsevier Ltd. This is an open access article under the CC BY-NC-ND license (http://creativecommons.org/licenses/by-nc-nd/4.0/).

Numerical models using finite element analysis (FEA) for existing structures have a total of six degrees of freedom (DOF) at each node (three translational and three rotational DOF). Therefore, a 6×6 FRF matrix with six DOF at an identical node as inputs and outputs has 36 FRF elements. Of these 36 elements, 27 (75% of the elements) involve rotational DOF in their inputs or outputs (hereinafter referred to as "rotational FRF").

On the other hand, conventional vibration tests obtain FRFs with only three translational DOF, resulting in experimental models with three translational DOF. Consequently, numerical models using FEA and experimental models have gaps in their DOF. These gaps lead to diverse problems. For example, previous studies have noted issues such as decreased analytical accuracy [9–16] in 1) transfer path analyses, which combine an experimental model obtained from vibration tests and a numerical model, and 2) projection of the dynamic characteristics in a combination system comprised of experimental and numerical models.

To address the issue above, several studies have examined rotational DOF measurement methods. These methods can be roughly classified into three types: (a) two-force excitation, (b) direct measurements of rotational FRFs, and (c) rotational FRF measurements using additional devices such as rigid blocks or transducers.

Type (a) includes methods to estimate a target structure's rotational FRFs based on the moment obtained by exciting multiple points located near an excitation point. Excitation can be induced using input devices such as two synchronized impact hammers or excitation devices [17–21]. Limitations of these methods include the size and shape of the target structure, location of the excitation points, and frequency range of the excitation on the target structure because two contact-type input devices must be installed on the target structure. In addition, it is difficult to completely synchronize the two input devices.

Type (b) includes 1) a method to install a microphone array at an arbitrary distance from the intended measurement point on the target structure to measure the rotational response at the measurement point [22], and 2) methods that use LDV or scanning LDV devices to measure the angular velocity at the measurement point [23–25]. Although these studies investigate methods that measure the angular velocity or the angular acceleration at points on the target structure in a non-contact manner, they do not apply a moment on the target structure in a non-contact manner as an input in a vibration test.

Type (c) includes methods to estimate the rotational FRFs of the target structure by installing additional structures (e.g., T-shaped metal blocks, cross-shaped metal blocks, PZT bimorph cantilevers, or six DOF transducers) to the measurement point in order to obtain the input–output relationship at the crossing point [26–35]. As these methods require the installation of additional structures, their applications and excitation frequencies are limited by the shape and size of these additional structures, the coupling method of the additional and target structures (adhesive or bolt fixing), and the rigidity of the coupling part.

Conventional vibration tests that use contact measurement devices are difficult to apply to microstructures (e.g., microelectromechanical systems), underwater structures, underwater robots, rotating structures, and structures in space. Although rotational FRF measurements using non-contact devices similar to type (b) have been examined, those using devices similar to types (a) and (c) have yet to be considered for non-contact measurements.

This study realizes a method to measure the rotational FRFs of a target structure by inputting a moment onto the excitation point of the target structure with a non-contact impulse excitation force induced by laser ablation (LA). LA is a phenomenon where a high-power pulse laser is irradiated on the surface of a target structure to form a plasma plume. Previously, we examined methods that employ LA for vibration and acoustic tests, and demonstrated the potential of LA in diverse fields [36–41]. LA is a technology that is used in driving micro air vehicles [42] and laser peening [43]. If LA generates an excitation force or moment that is an ideal impulse, the Fourier spectrum of the measured response corresponds to the FRF. Therefore, input-detection-free rotational FRF measurements can be realized using LA as an input [36].

Our method splits a laser beam so that LA occurs simultaneously at multiple points, which are located near the excitation point of the target structure, effectively applying the moment to the excitation point. Even if there is a several-meter difference in the distance between the point of diversion in the laser beam and their respective LA occurrence points, the timing of LA occurrence at both points can be considered simultaneous by taking the velocity of light into account. This study measures the rotational FRFs where the moment is the input and the velocity is the output. The resulting FRFs are compared to those obtained using FEA. In addition, the influence of random errors within the measured rotational FRFs is evaluated using reliability coefficients [47]. Furthermore, the modal vectors of the FRFs obtained by the proposed method and FEA are compared and evaluated quantitatively using the modal assurance criterion (MAC) to demonstrate the efficacy of our method.

2. Principle of LA moment excitation

LA is a phenomenon where a pulsed laser beam is irradiated on a solid object such that a plasma plume is released from its surface in an explosive way (Fig. 1). When a plasma plume with a mass of Δm is released from the surface with a velocity of v, the momentum (impulse) becomes Δmv. This is the excitation input to the target structure. The excitation force provided by LA acts along the direction of the normal line of the target structure. Consequently, the force is independent of the incident angle of the laser beam to the excited surface [36–41].

Fig. 2 shows the principle for inputting the moment to the target structure. The moment acting on the target structure is M, the excitation forces applied on points 1 and 2 are F_1 and F_2, respectively, and the distance between the excitation points is d. When $F_1 = F_2 = F$, M is expressed as

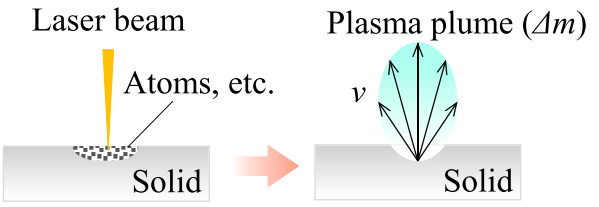

Fig. 1. Laser ablation.

$$M = \frac{1}{2}(F_1 + F_2) = Fd \tag{1}$$

Champoux et al. [18] provided F_1 and F_2 using impulse hammers. In our method, F_1 and F_2 are applied by LA.

3. Rotational FRFs

3.1. LA moment excitation system

Fig. 3 is an overview of our LA moment excitation system. This system converts the laser beam of linearly polarized light emitted from an Nd:YAG pulse laser (Surelite III-10, Continuum; wavelength, 1064 nm; laser beam diameter, 9.5 mm; pulse width, 5 ns; maximum output, 850 mJ; radial divergence angle, 0.45 mrad) into circularly polarized light using a λ/4 wave plate (quartz waveplate WPQ-10640-4 M, Sigma Koki). The laser beam is dispersed using a half mirror (laser line plate half mirror PSMH-30C03-10-1064, Sigma Koki). The laser pulse energy is equally divided. Then, the two dispersed laser beams are focused using a plano-convex lens (plano convex lenses SLB-30-100P, Sigma Koki) via a mirror (laser line mirrors TFM-30C05-1064, Sigma Koki). LA occurs simultaneously at two sides of the test piece (size: 120 mm × 50 mm, plate thickness: 3 mm), and the moment excitation is in the direction with angle of θ_y to the test piece.

The time required for the two dispersed laser beams to excite the test piece differs due to the different courses; one is reflected on the half mirror while the other passes through the mirror. However, this time difference may be ignored considering the velocity of light ($c \approx 3 \times 10^8$ m/s). The angle between the laser beams and the surface of the excited test piece is 45°.

Data processing was conducted by measuring the velocity response in the z-direction using a LDV (NLV-2500-5, Polytec) and analyzing the frequency responses (Fourier spectrum) using a spectrum analyzer (A/D, NI PXI-4462, National Instruments; software, Catec, CAT-System). In this measurement, the sampling frequency, number of sampling points, and average count are 102.4 kHz, 32768, and 10, respectively. After approximately 100 ns of a transistor-transistor logic (TTL) signal from the pulsed-laser system, a laser beam is irradiated. Once the spectrum analyzer receives the TTL signal, it starts to measure the response from the preceding 0.01 s.

3.2. Test piece

Fig. 4 illustrates the test piece, which is a 5052 aluminum alloy plate measuring 120 mm × 50 mm × 3 mm. Its boundary conditions are similar to a cantilever where only one end is fixed. In this study, the moment is applied on each excitation point: A and B. To apply the moment to point A (B), LA was made simultaneously at points A_1 and A_2 (B_1 and B_2).

To obtain the modal vectors of the rotational DOF, a finite element model for the test piece with 1-mm mesh size shell elements was created. Then eigenvalue analysis using FEA (NASTRAN) was performed to obtain the natural frequencies and modal vectors.

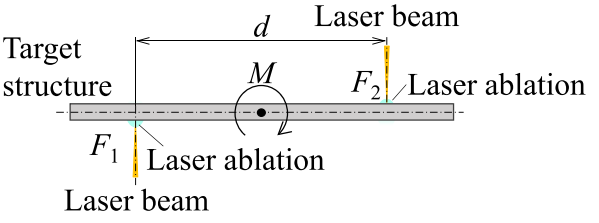

Fig. 2. Laser ablation moment excitation force.

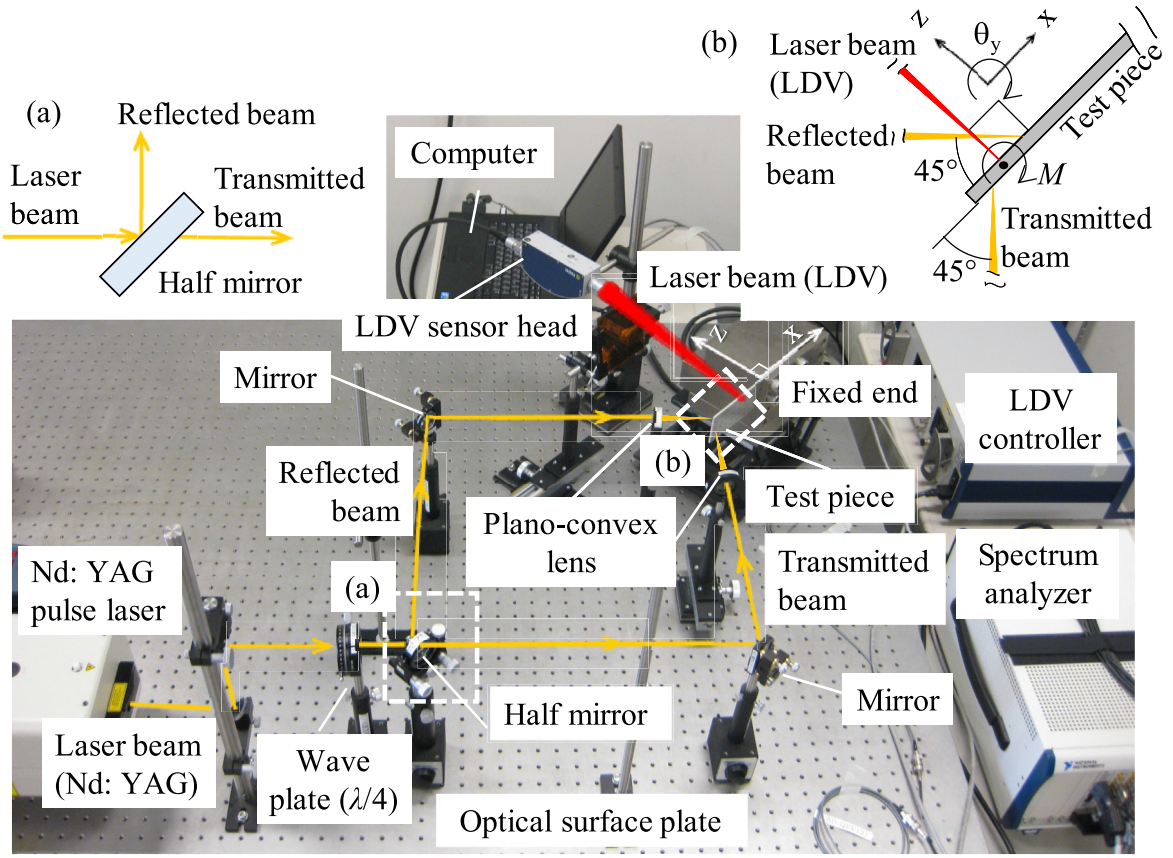

Fig. 3. Laser ablation moment excitation system for non-contact vibration tests.

3.3. *Measurements of the rotational FRFs based on LA moment excitation*

3.3.1. *Estimation of LA moment excitation based on Newton's second law of motion*

This section estimates the excitation force generated by LA using Newton's second law [36]. Equation (1) represents the magnitude of LA moment excitation. Fig. 5 shows the LA excitation force estimation system. A cube with mass m [kg], whose size and materials can be considered rigid within the frequency scope to be measured, was suspended on a string. This creates

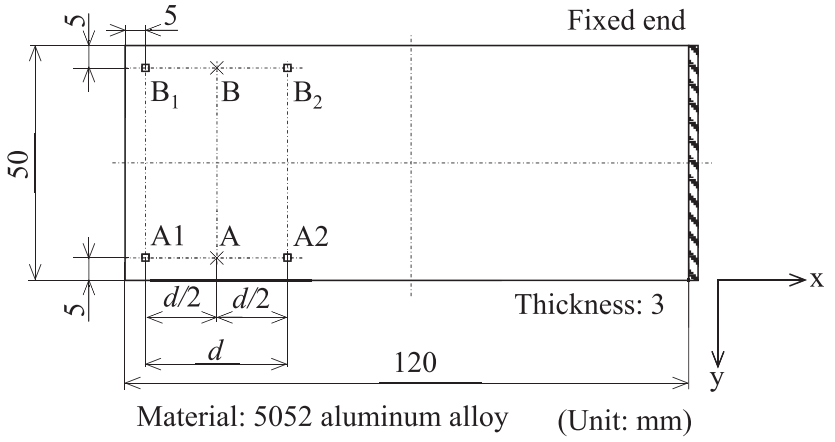

Fig. 4. Excitation and measurement points of the test piece.

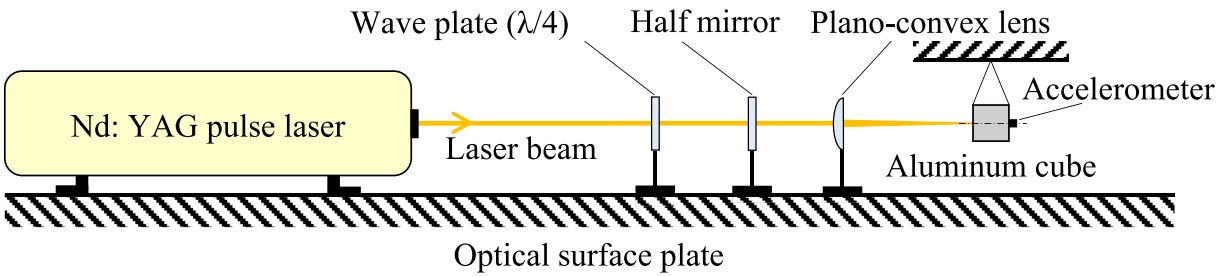

Fig. 5. Estimation of the laser excitation force using the rigid body pendulum method.

a free-free boundary condition (hereinafter referred to as a rigid-body pendulum). The acceleration of the cube $a(\omega)$ [m/s^2] was calculated by measuring the time history of the response of the rigid body's acceleration when LA occurs on the cube and performing a Fourier transformation of the response. The LA excitation force can be obtained using Newton's second law, $F(\omega) = ma(\omega)$.

If the LA excitation force is considered to be an ideal impulse, $F(\omega)$ assumes a constant value and the LA excitation force F is obtained as a scalar value by averaging the values of $F(\omega)$ within the frequencies to be measured. The Fourier spectrum of $F(t)$ should theoretically be a real constant value over the range of frequencies because a LA excitation force can be considered an ideal impulse. Therefore, $|F(\omega)|$, which is the absolute value of the Fourier spectrum of the LA excitation force $F(t)$, can be averaged to obtain the scalar value of the LA excitation force F.

For operations under identical conditions (e.g., the same target material, laser fluence, atmospheric pressure, ambience, etc.), LA can be assumed to be the same. Therefore, if LA excitations (LA moment excitation) in a rigid-body pendulum and in vibration tests are applied under the same conditions, our method is valid. Only the response of the target structure has to be experimentally measured if the LA excitation force (moment) is measured in advance.

In this experiment, a cube with 20-mm sides composed of a 5052 aluminum alloy, which is the same material as the test piece, was used for the rigid-body pendulum. Laser beams were irradiated along the central axis so that the responses were measured by an accelerometer attached directly behind the LA occurrence point. To estimate the LA excitation force, the optical elements were set so that the beam course was the same as that of the FRF measurement using LA moment excitation (see Fig. 3).

Fig. 6(a) and (b) respectively show the time history waveform of the measured acceleration responses of the cube and the Fourier transformation of the time history waveform when the laser pulse energy is 425.9 mJ. The sampling frequency, number of sampling points, and average count in the measurement are the same as those in Section 3.1. Fig. 6(a), which shows an enlargement of the period of 0 s–0.1 s, indicates that LA realizes an ideal impulse excitation force on the cube. The

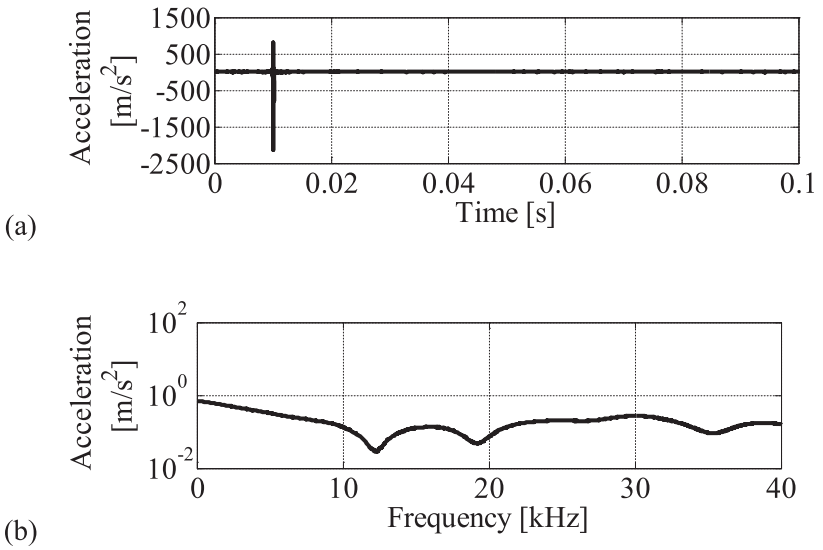

Fig. 6. Measured LA excitation force for a 20-mm aluminum cube when the laser pulse energy is set at 425.9 mJ. (a) Time response and (b) average Fourier spectrum corresponding to (a).

magnitude of the amplitude of the Fourier spectrum is almost constant until 40 kHz (Fig. 6(b)). However, cube dynamics may be influenced by natural frequencies above 40 kHz as well as accelerometer attached to the cube. Consequently, the absolute value of the Fourier spectrum's amplitude of the LA excitation force changes slightly.

The magnitude of LA moment excitation M can be controlled by changing d or F in Eq. (1). This study controls F by changing the energy of the dispersed laser pulse to 182.2 mJ, 227.7 mJ, 327.3 mJ, or 425.9 mJ. d is changed to 5 mm, 10 mm, 20 mm, or 30 mm. Thus, M has a total of 16 patterns.

Although the components of the impulse excitation force generated by LA are sustained until 40 kHz (Fig. 6(b)), the measurement range is up to 10 kHz after considering the relationship between the wavelength in the vibrational mode shapes of the test piece and d. Accordingly, when the laser pulse energy is 182.2 mJ, 227.7 mJ, 327.3 mJ, and 425.9 mJ, F is 1.08 mN, 1.62 mN, 3.24 mN, and 6.48 mN, respectively, by averaging the absolute values of the Fourier spectrum to 10 kHz.

3.3.2. Procedure for input-detection-free rotational FRF measurements

The test piece's auto rotational FRF at point A and the cross rotational FRFs between points A and B were measured using the LA moment excitation system (Fig. 2). Initially, the velocity response $v_{\mathrm{struct}}(t)$ when LA moment excitation occurred at point A or B was evaluated using a LDV. The obtained Fourier spectrum of the velocity response $v_{\mathrm{struct}}(\omega)$ was divided by M, which was estimated in advance (See section 3.3.1.). Subsequently, the dead time contained in the measurement was corrected for the obtained FRFs. Here, the dead time refers to the difference between the time when the test piece actually starts to respond and the time when the spectrum analyzer starts the measurement. If the input and response have the same dead time, the dead time is nullified. In our method, the dead time must be considered because the proposed method measures the FRFs based only on the responses. As discussed above, correcting the absolute values and phase characteristics of the Fourier spectrum realizes an input-detection-free rotational FRF measurement.

3.3.3. Reliability factor

Based on the concept of coherence functions, this section evaluates the reliability of the FRFs measured by the proposed method using a reliability coefficient [47]. The coherence function $\gamma^2(\omega)$ can be defined by the following equations

$$\gamma^2(\omega) = \frac{\left|G_{\mathrm{Input-Output}}(\omega)\right|^2}{G_{\mathrm{Input}}(\omega)\ G_{\mathrm{Output}}(\omega)} \tag{2}$$

$$G_{\mathrm{Input}}(\omega) = \frac{1}{N}\sum_{i=1}^{N}\left|G^{(i)}_{\mathrm{Input}}(\omega)\right|^2 \tag{3}$$

$$G_{\mathrm{Output}}(\omega) = \frac{1}{N}\sum_{i=1}^{N}\left|G^{(i)}_{\mathrm{Output}}(\omega)\right|^2 \tag{4}$$

$$G_{\mathrm{Input-Output}}(\omega) = \frac{1}{N}\sum_{i=1}^{N}\left|G^{(i)}_{\mathrm{Input-Output}}(\omega)\right|^2 \tag{5}$$

Here, $G_{\mathrm{Input}}(\omega)$, $G_{\mathrm{Output}}(\omega)$, $G_{\mathrm{Input\text{-}Output}}(\omega)$, and N refer to the power spectrum of the input , power spectrum of the output, cross spectrum between the inputs and outputs, and trial counts, respectively. In this system, the input is a constant value independent of the frequency. Thus, Eq. (3) is redefined as

$$G_{\mathrm{Input}}(\omega) \equiv G_{\mathrm{M}} \tag{6}$$

Subsequently, Eq. (6) can be substituted into Eq. (2) to define $R^2(\omega)$ as

$$R^2(\omega) \equiv \frac{\left|G_{\mathrm{M-Output}}(\omega)\right|^2}{G_{\mathrm{M}}G_{\mathrm{Output}}(\omega)} \tag{7}$$

Strictly speaking, $R^2(\omega)$ differs from $\gamma^2(\omega)$. However, its value ranges $0 \le R^2(\omega) \le 1$. When the value of R^2 is closer to 1, the impact of random noise contained in the rotational FRF decreases.

3.4. Auto and cross rotational FRFs

Figs. 7 and 8 show the auto rotational FRF ($H_{\mathrm{Az-A\theta y}}$) and the cross rotational FRFs ($H_{\mathrm{Bz-A\theta y}}$ and $H_{\mathrm{Az-B\theta y}}$) between points A and B, respectively. The magnitude of LA moment excitation used to obtain the FRFs is set to 0.0324 mN·m upon considering the LA excitation force is $F = 1.08$ mN (laser pulse energy: 182.2 mJ) obtained in Section 3.3.1 and the distance between the excitation points is $d = 30$ mm. Fig. 9 shows the auto translational FRF ($H_{\mathrm{Az-Az}}$) at point A when the LA excitation force is

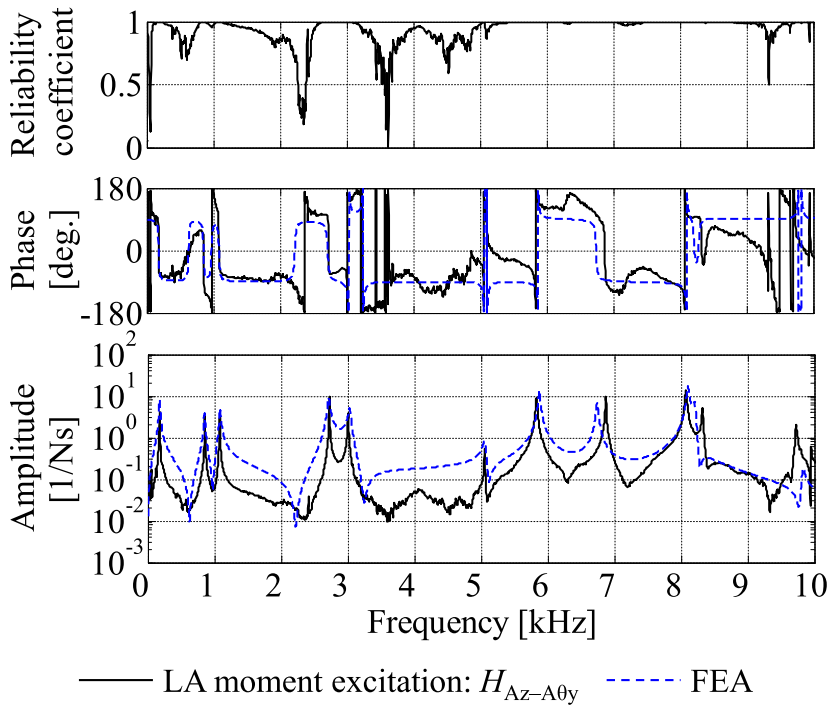

Fig. 7. Reliability coefficient, phase, and amplitude of the auto rotational FRF ($H_{Az-A\theta y}$) measured by LA moment excitation (black solid line) and FEA (blue dashed line). LA excitation force F is 1.08 mN when the laser pulse energy is set to 182.2 mJ and the distance between excitation points d is 30 mm. Therefore, the amplitude of LA moment excitation is 0.0324 mN m. (For interpretation of the references to colour in this figure legend, the reader is referred to the Web version of this article.)

$F = 1.08$ mN (laser pulse energy: 182.2 mJ). For comparison, Figs. 7–9 show the FRFs obtained with FEA. Each figure also presents the reliability coefficients, FRFs' phase characteristics, and amplitudes of their absolute value.

The modal damping ratios of the FRF obtained with FEA were set as follows: 4% for the 1st, 1% for 2nd and 3rd, 0.6% for 4th and 5th, 0.4% for 6th, and 0.2% for 7th and higher. The modal damping ratios were empirically estimated by fitting the calculated FRFs by FEA with those obtained in the experiment. Table 1 shows the natural frequencies obtained by this experiment and FEA. The FRFs measured in this experiment agree well with those obtained by FEA with respect to their phase characteristics and amplitudes of the absolute values. However, their amplitudes in non-resonant areas disagree.

The reliability coefficients in Figs. 7–9 show similar tendencies as the coherence function. That is, the coefficients are close to 1 at a resonant point but decrease at an antiresonant point. The reliability coefficient decreases in the lower frequency range below 5 kHz because the small magnitude of the input degrades the accuracy of the measured response in the low frequency range. This suggests that the accuracy of the rotational FRF measured in this study can be evaluated using reliability coefficients. The cross FRFs ($H_{Bz-A\theta y}$ and $H_{Az-B\theta y}$ in Fig. 8) agree well with each other, implying a linear system process.

Subsequently, the vibrational mode shapes were obtained by identifying the modal parameters of the measured 45 rotational FRFs using the multi-point differential iteration method. The vibrational mode shapes in the proposed method and FEA were obtained to compare their modal vectors using the MAC.

$$\mathrm{MAC}(\phi_{FEA},\ \phi_{EXP}) = \frac{\left|\{\phi_{FEA}\}^T\{\phi_{EXP}\}\right|^2}{\left(\{\phi_{FEA}\}^T\{\phi_{EXP}\}\right)\left(\{\phi_{EXP}\}^T\{\phi_{FEA}\}\right)} \tag{8}$$

Here φ_{FEA} and φ_{EXP} refer to the modal vector obtained by FEA and that measured in this experiment, respectively. Fig. 10 shows the vibrational mode shapes of the 1st to 11th modes.

Table 2 lists the MAC values. These two FRFs' vibrational mode shapes agree with each other. Table 2 also shows that up to 9th mode, the MAC value is about 0.9, suggesting that the modal vectors are almost the same. In the 10th and 11th modes, the MAC values decrease slightly, which may be related to the wavelength of vibrational mode shape and the distance between the excitation points. Champoux et al. [18] reported that the estimated accuracy of the rotational FRF is affected by the distance between excitation points. The results of this study agree well with Champoux et al. [18].

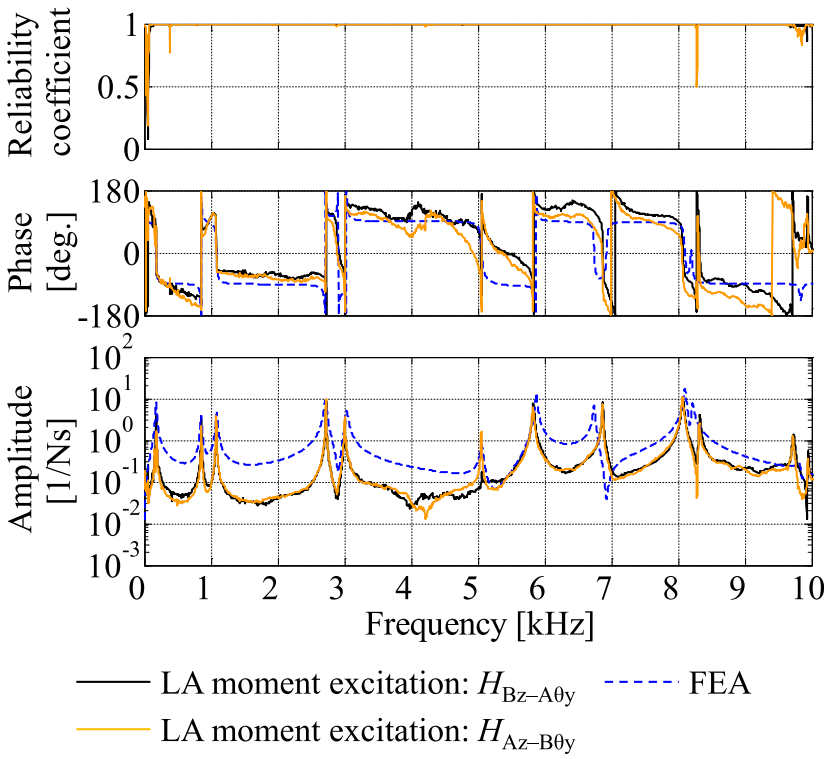

Fig. 8. Reliability coefficient, phase, and amplitude of the cross rotational FRF ($H_{Bz–A\theta y}$: black solid line, $H_{Az–B\theta y}$: orange solid line) measured by LA moment excitation and FEA (blue dashed line). LA excitation force F is 1.08 mN when the laser pulse energy is set to 182.2 mJ and the distance between excitation points d is 30 mm. Therefore, the amplitude of LA moment excitation is 0.0324 mN m. (For interpretation of the references to colour in this figure legend, the reader is referred to the Web version of this article.)

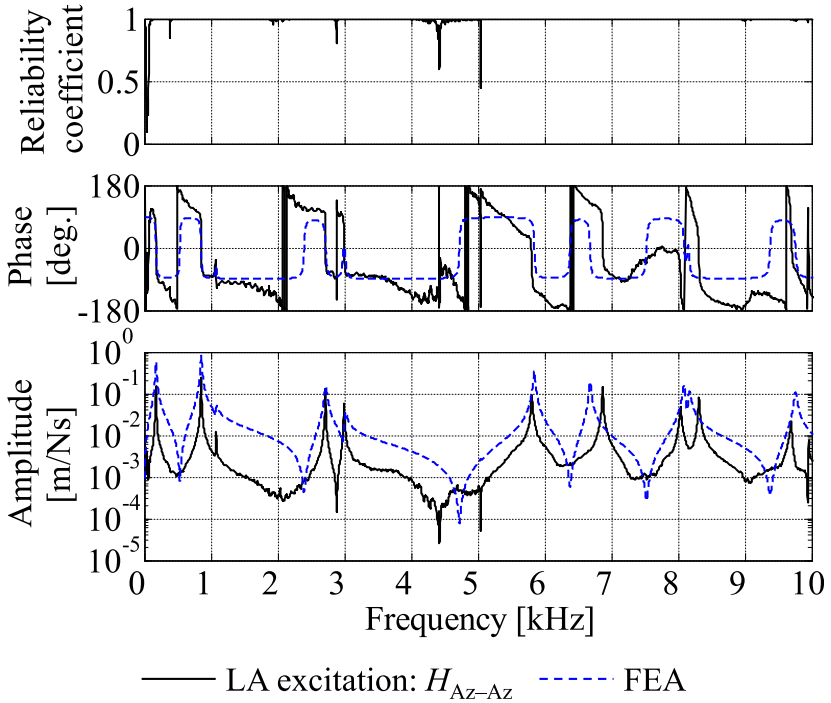

Fig. 9. Reliability coefficient, phase, and amplitude of the auto translational FRF ($H_{Az–Az}$) measured by LA excitation force (black solid line) and FEA (blue dashed line). LA excitation force F is 1.08 mN when the laser pulse energy is set to 182.2 mJ. (For interpretation of the references to colour in this figure legend, the reader is referred to the Web version of this article.)

Table 1
Natural frequencies of the test piece.

Natural frequency [Hz]			
Mode	FEA	Experiment	Error
1st	173	172	−0.6
2nd	850	849	−0.1
3rd	1075	1075	0.0
4th	2715	2712	−0.1
5th	3009	2992	−0.6
6th	5053	5034	−0.4
7th	5841	5807	−0.6
8th	6677	6865	2.8
9th	8084	8037	−0.6
10th	8161	8310	1.8
11th	9754	9725	−0.3

3.5. Effect on the accuracy of the rotational FRFs

This section examines the effects of the distance between excitation points d on the accuracy of the rotational FRFs. Initially, the rotational FRFs were measured as d changed from 5 mm, 10 mm, 20 mm, to 30 mm. Here, the measured rotational FRFs are the auto FRFs at point A and the LA excitation force is $F = 1.08$ mN (laser pulse energy: 182.2 mJ). Figs. 11–13 show the rotational FRFs with $d = 5$ mm, 10 mm, and 20 mm, respectively. For comparison, the FRFs from FEA are also shown. The natural frequencies of the FRFs agree well with each other and are independent of the magnitude of M. However, near the antiresonance point, when M increases (d increases), the absolute values of the rotational FRFs approach those of the FRF obtained with FEA, and the reliability coefficients of the rotational FRF are enhanced, suggesting improved accuracy. In addition, the phase characteristics also become the correct values at the resonance point. However, when comparing the case with $d = 20$ mm (Fig. 13) to that with $d = 30$ mm (Fig. 7), the absolute values of the FRFs, phase characteristics, and reliability coefficients are similar. In particular, the case with $d = 30$ mm measures the antiresonance point more precisely near 3.6 kHz compared to that with $d = 20$ mm. Accordingly, the decrease in the values of the reliability coefficients can be observed at the antiresonance point. In our method, the accuracy of the rotational FRF increases by increasing M due to the increased signal-to-noise (SN) ratio.

Next, the more significant contributor (F or d) to the increased accuracy of the rotational FRF was examined. Figs. 14–16 show the rotational FRFs obtained when adjusting F and d so that the magnitude of M is identical (0.0324 mN·m). For comparison, the rotational FRFs obtained by FEA are also shown. In Figs. 14–16, the natural frequencies obtained in our experiment and FEA agree well with each other and are independent of the magnitude of M. Additionally, when the magnitude of M is identical, d contributes more significantly to the enhanced accuracy of the rotational FRFs than F. As d increases, antiresonance points appear at 2.5 kHz, 3.5 kHz, and 9.3 kHz. The reliability coefficients decrease near these points. These tendencies are the same to those observed in Figs. 11–13. Therefore, for an identical F or M, increasing d results in a more accurate FRF. However, there are some constraints on d due to vibrational mode shape of the target structure. Although using a larger M via a larger F and larger d may provide a more accurate rotational FRF, we could not demonstrate this result using a larger F due to our pulsed-laser system and optical system.

4. Conclusions

This study examines a non-contact measurement method for rotational FRFs using an impulse excitation force where the moment is the input and the velocity is the output. A laser beam radiated from an Nd:YAG pulse laser emitter is dispersed using a half mirror to halve the laser pulse energy. Then, radiating the laser beams onto two points near an excitation point on the target structure simultaneously generates LA, and the moment is applied onto the target structure in a non-contact manner. Similar to our previously reported input-detection-free FRF measurements [36], the proposed method obtains rotational FRFs by dividing the Fourier spectrum measured during LA moment excitation by the magnitude of LA moment excitation. The excitation is estimated using Newton's second law and subsequently corrected for the dead time in the measurement.

The experiment used a 5052 aluminum alloy plate where one end was fixed as the test piece. The auto FRFs and cross FRFs on the rotational degrees of freedom between arbitrary points on the test piece were measured. The experimental FRFs and those obtained by FEA agree well, indicating that our method can realize an input-detection-free measurement of the rotational DOF FRF.

The relationship between the accuracy of the rotational FRFs measured by our method and the magnitude of LA moment excitation was examined. When the magnitude of the laser pulse energy (LA excitation force) is identical, increasing the distance between excitation points, which controls the magnitude of LA moment excitation, improves the agreement

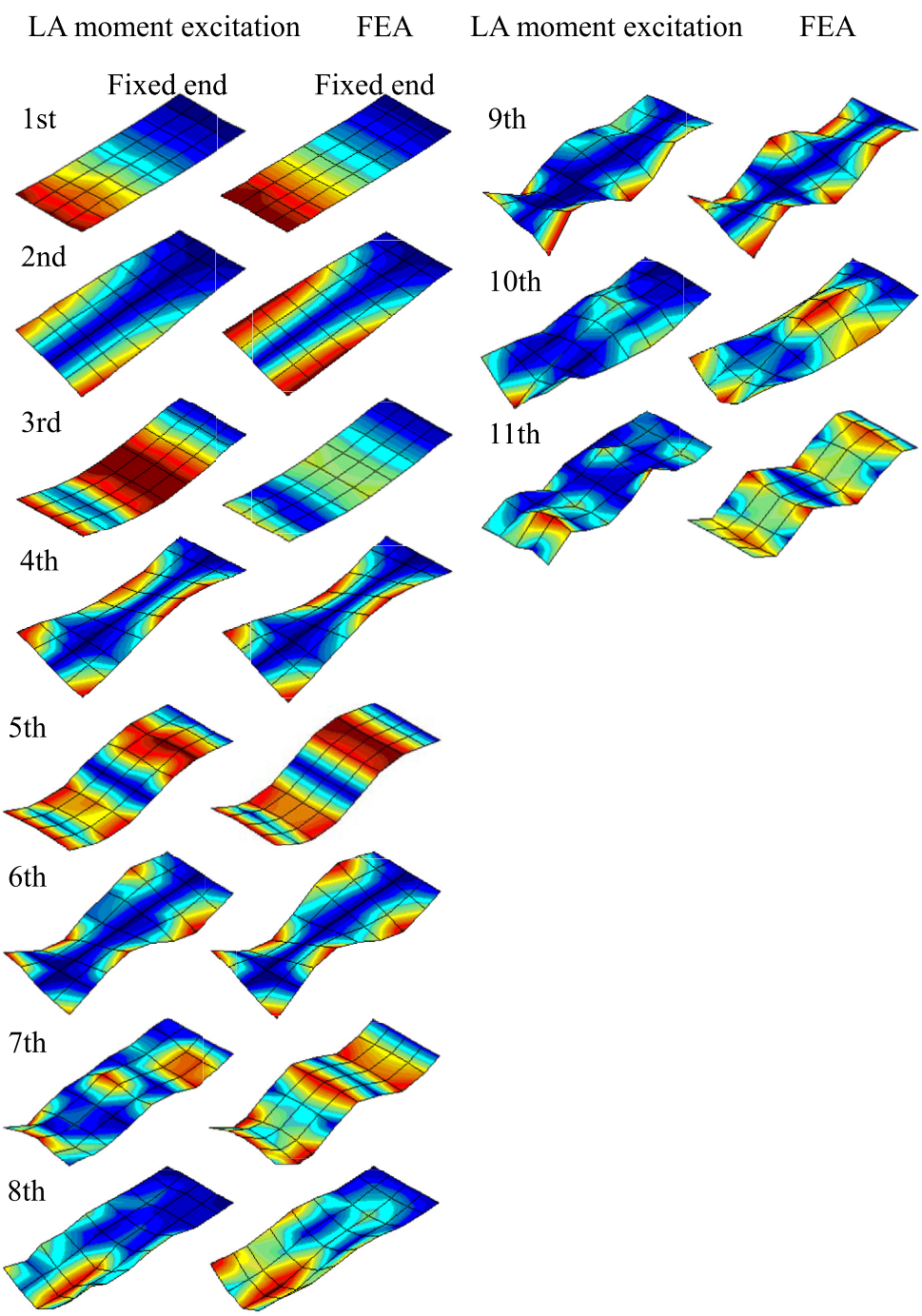

Fig. 10. Mode shapes up to 10 kHz for the test piece identified from the measured rotational FRFs during LA moment excitation and FEA. LA excitation force F is 1.08 mN when the laser pulse energy is set to 182.2 mJ and the distance between the excitation points d is 30 mm. Therefore, the amplitude of LA moment excitation is 0.0324 mN·m.

between the FRFs measured by the proposed method and those obtained by FEA. In addition, when the laser pulse energy and the distance between excitation points are varied while applying an identical LA moment excitation force, changes in the latter enhance the agreement between the measured FRFs and those obtained by FEA.

The accuracy of the rotational FRFs and the measurable frequency range were evaluated by calculating MAC between the modal vectors obtained by the proposed method and those obtained by FEA. When the distance between excitation points is 30 mm (the magnitude of LA excitation moment is 0.0324 mN·m), the MAC value is 0.9 for a frequency range up to 8 kHz. To

Table 2
MAC values between modal vectors identified from the measured rotational FRFs during LA moment excitation and those obtained by FEA.

Mode	Measured natural frequency [Hz]	MAC
1st	172	0.97
2nd	849	1.00
3rd	1075	1.00
4th	2712	0.98
5th	2992	0.98
6th	5034	0.96
7th	5807	0.90
8th	6865	0.90
9th	8037	0.86
10th	8310	0.83
11th	9725	0.73

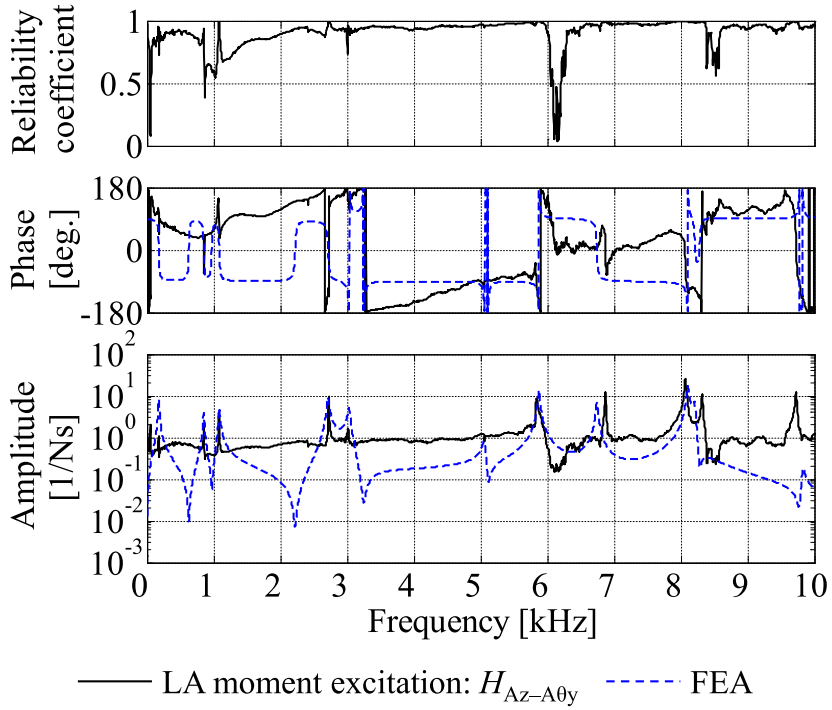

Fig. 11. Reliability coefficient, phase, and amplitude of the auto rotational FRF ($H_{Az-A\theta y}$) measured by LA moment excitation (black solid line) and FEA (blue dashed line). LA excitation force F is 1.08 mN when the laser pulse energy is set to 182.2 mJ and the distance between excitation points d is 5 mm. Therefore, the amplitude of LA moment excitation is 0.0054 mN m. (For interpretation of the references to colour in this figure legend, the reader is referred to the Web version of this article.)

measure the rotational FRFs precisely, it is important to increase the magnitude of LA moment excitation and to increase the distance between the excitation points. Moreover, to extend the measurable frequency range of the proposed method above 8 kHz, the distance between the excitation points must be decreased. Because the distance between these points is also related to the accuracy of the rotational FRFs, the distance should be set appropriately by considering the size of the target structure and experimental conditions. Furthermore, to expand the proposed method in an effort to realize non-destructive and non-contact FRF measurements using laser excitations, LA should be replaced with laser-induced plasma shock waves [44–50].

The proposed method may be applicable to numerous structures, including microstructures, underwater structures, underwater robots, rotating structures, and space structures in the future. Furthermore, the proposed method may realize other uses such as transfer path analysis with rotational DOFs, damage detection based on vibrational modes obtained by moment excitation, and dynamic prediction using rotational FRFs. Furthermore, if LA moment excitation device can be field-

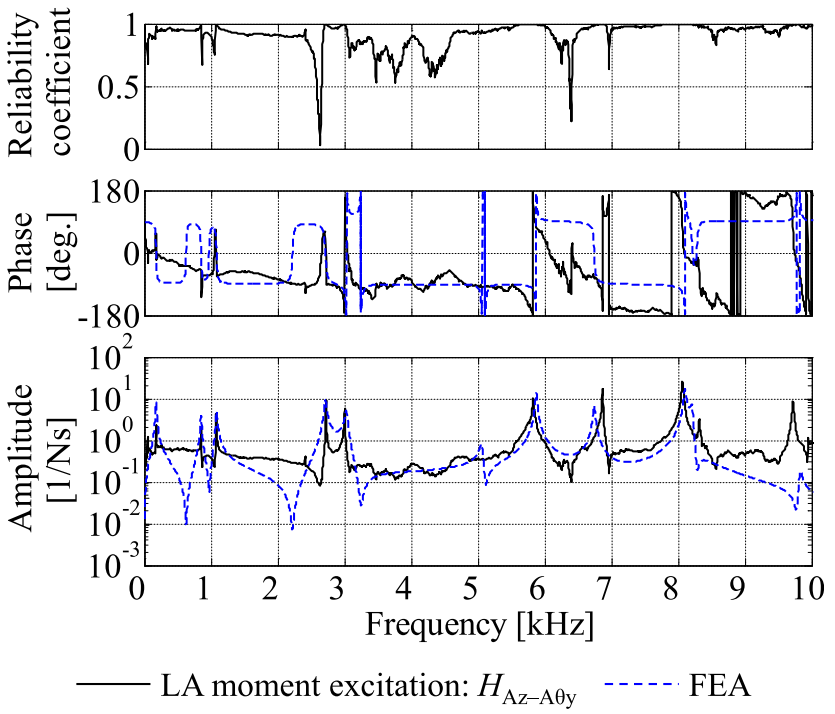

Fig. 12. Reliability coefficient, phase, and amplitude of the auto rotational FRF ($H_{\mathrm{Az-A\theta y}}$) measured by LA moment excitation (black solid line) and FEA (blue dashed line). LA excitation force F is 1.08 mN when the laser pulse energy is set to 182.2 mJ and the distance between excitation points d is 10 mm. Therefore, the amplitude of LA moment excitation is 0.0108 mN m. (For interpretation of the references to colour in this figure legend, the reader is referred to the Web version of this article.)

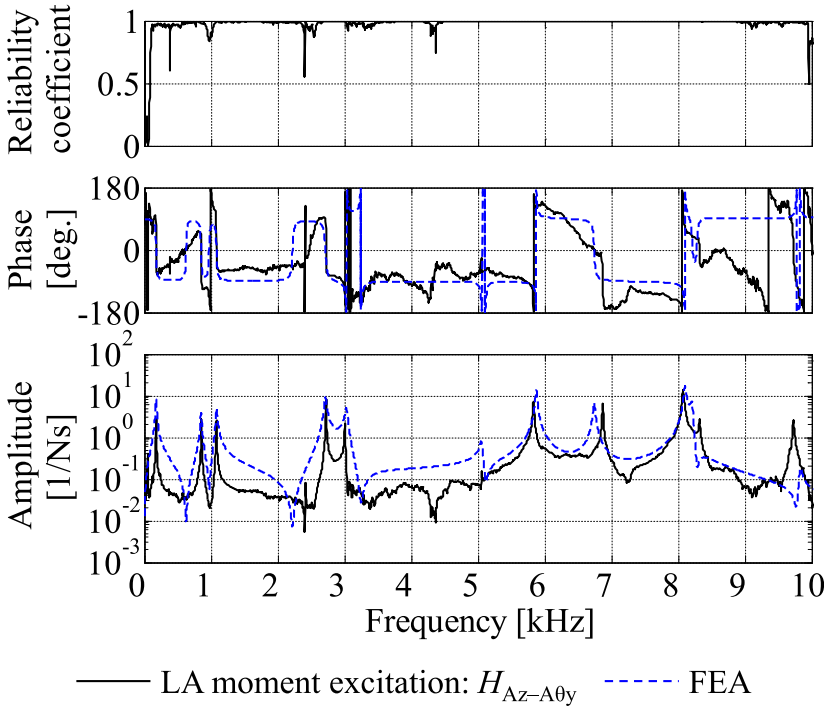

Fig. 13. Reliability coefficient, phase, and amplitude of the auto rotational FRF ($H_{\mathrm{Az-A\theta y}}$) measured by LA moment excitation (black solid line) and FEA (blue dashed line). LA excitation force F is 1.08 mN when the laser pulse energy is set to 182.2 mJ and the distance between excitation points d is 20 mm. Therefore, the amplitude of LA moment excitation is 0.0216 mN m. (For interpretation of the references to colour in this figure legend, the reader is referred to the Web version of this article.)

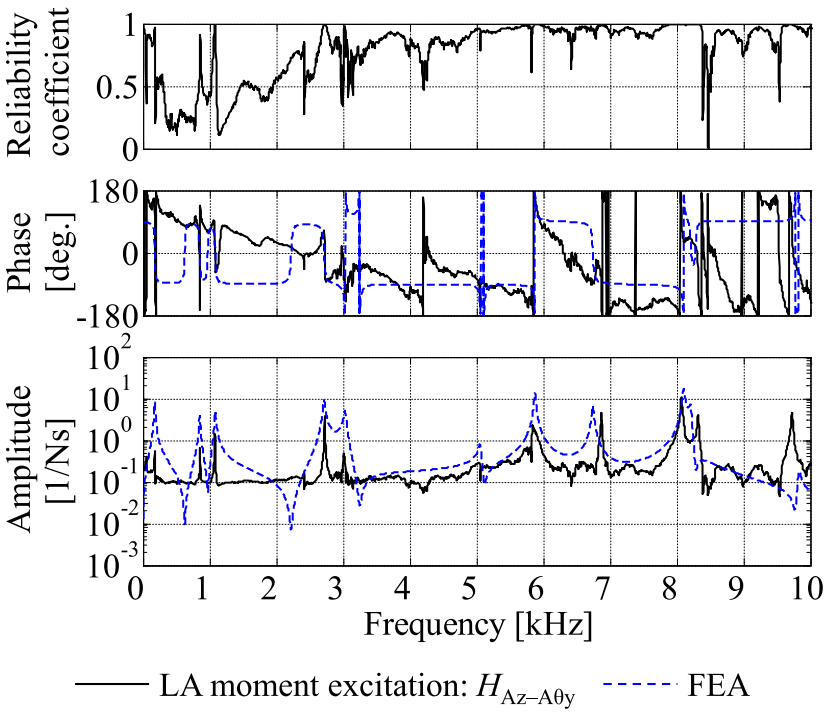

Fig. 14. Reliability coefficient, phase, and amplitude of the auto rotational FRF ($H_{\mathrm{Az-A\theta y}}$) measured by LA moment excitation (black solid line) and FEA (blue dashed line). LA excitation force F is 6.48 mN when the laser pulse energy is set to 425.9 mJ and the distance between excitation points d is 5 mm. Therefore, the amplitude of LA moment excitation is 0.0324 mN m. (For interpretation of the references to colour in this figure legend, the reader is referred to the Web version of this article.)

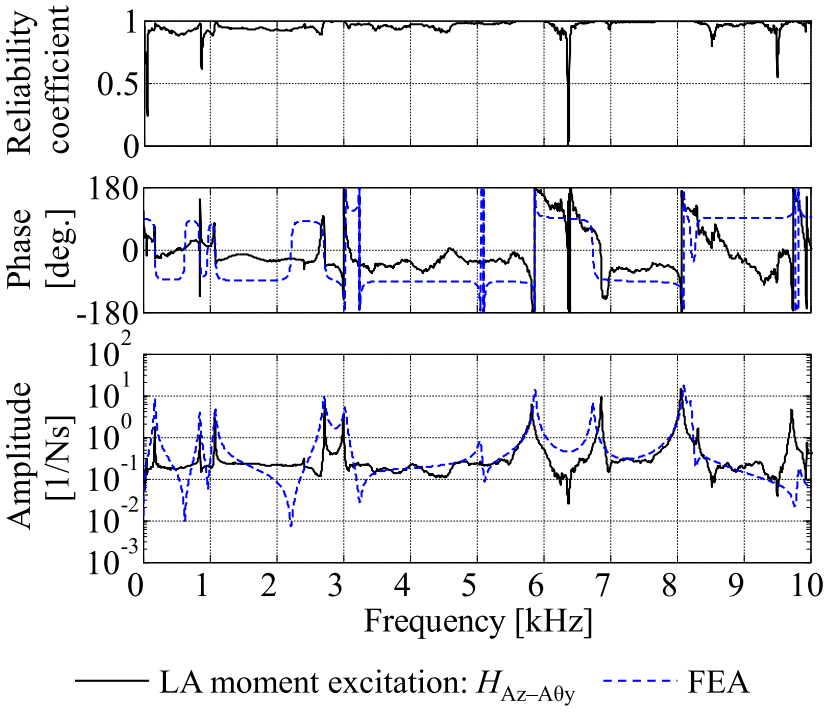

Fig. 15. Reliability coefficient, phase, and amplitude of the auto rotational FRF ($H_{\mathrm{Az-A\theta y}}$) measured by LA moment excitation (black solid line) and FEA (blue dashed line). LA excitation force F is 3.24 mN when the laser pulse energy is set to 327.3 mJ and the distance between excitation points d is 10 mm. Therefore, the amplitude of LA moment excitation is 0.0324 mN m. (For interpretation of the references to colour in this figure legend, the reader is referred to the Web version of this article.)

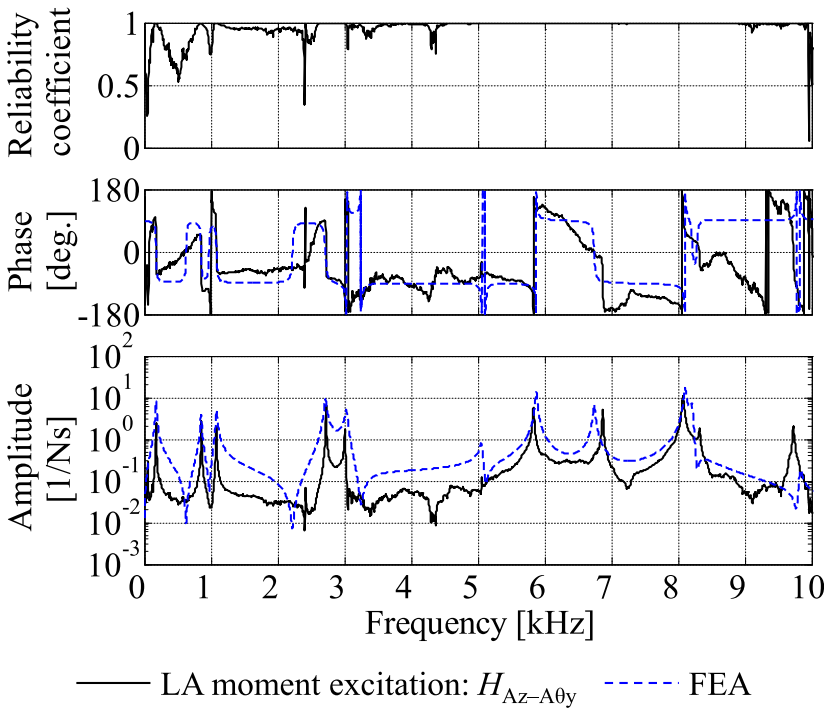

Fig. 16. Reliability coefficient, phase, and amplitude of the auto rotational FRF ($H_{\mathrm{Az-A\theta y}}$) measured by LA moment excitation (black solid line) and FEA (blue dashed line). LA excitation force F is 1.62 mN when the laser pulse energy is set to 227.7 mJ and the distance between excitation points d is 20 mm. Therefore, the amplitude of LA moment excitation is 0.0324 mN m. (For interpretation of the references to colour in this figure legend, the reader is referred to the Web version of this article.)

portable, our method will be an user-friendly device such as an impulse hammer in general vibration tests, and this is our future work.

Declaration of conflicting interests

The authors certify that there is no conflict of interest with the Japan Society for the Promotion of Science.

Acknowledgments

We thank the Japan Society for the Promotion of Science for support under Grants-in-Aid for Scientific Research programs (Grants-in-Aid for Scientific Research (B), Project No. JP16H04291 and No. JP16H04286, and Grant-in-Aid for Challenging Exploratory Research, Project No. JP17K18858).

References

[1] D.J. Ewins, Modal Testing: Theory, Practice and Application, second ed., Research Studies Press Ltd., Pennsylvania, 2000.
[2] K.G. McConnel, P.S. Varoto, Vibration Testing: Theory and Practice, second ed., John Wiley & Sons Inc., New Jersey, 2008.
[3] J.M.M. Silva, N.M.M. Maia, A.M.R. Ribeiro, Cancellation of mass-loading effects of transducers and evaluation of unmeasured frequency response functions, J. Sound Vib. 236 (2000) 761–779.
[4] S.A. Sands, P. Camilleri, R.A. Breuer, G.K. Cambrell, R.J. Alfredson, E.M. Skuza, P.J. Berger, M.H. Wilkinson, A novel method for the measurement of mechanical mobility, J. Sound Vib. 320 (2009) 559–575.
[5] M. Wang, D. Wang, G. Zheng, Joint dynamic properties identification with partially measured frequency response function, Mech. Syst. Signal Process. 27 (2012) 499–512.
[6] S. Bi, J. Ren, W. Wang, G. Zong, Elimination of transducer mass loading effects in shaker modal testing, Mech. Syst. Signal Process. 38 (2013) 265–275.
[7] B. Bediz, E. Korkmaz, O.B. Ozdoganlar, An impact excitation system for repeatable, high-band width modal testing of miniature structures, J. Sound Vib. 333 (2014) 2743–2761.
[8] N. Hosoya, S. Yaginuma, H. Onodera, T. Yoshimura, Estimation of the auto frequency response function at unexcited points using dummy masses, J. Sound Vib. 337 (2015) 14–27.
[9] S.S. Park, Y. Altintas, M. Movahhedy, Receptance coupling for end mills, Int. J. Mach. Tool Manuf. 43 (2003) 889–896.
[10] T. Yang, S.H. Fan, C.S. Lin, Joint stiffness identification using FRF measurements, Comput. Struct. 81 (2003) 2549–2556.
[11] K.Y. Sanliturk Cakar, Elimination of transducer mass loading effects from frequency response functions, Mech. Syst. Signal Process. 19 (2005) 87–104.
[12] D. Čelič, M. Boltežar, Identification of the dynamic properties of joints using frequency–response functions, J. Sound Vib. 317 (2008) 158–174.
[13] D. Čelič, M. Boltežar, The influence of the coordinate reduction on the identification of the joint dynamic properties, Mech. Syst. Signal Process. 23 (2009) 1260–1271.

[14] A.T. Moorhouse, T.A. Evans, A.S. Elliott, Some relationships for coupled structures and their application to measurement of structural dynamic properties in situ, Mech. Syst. Signal Process. 25 (2011) 1574–1584.
[15] M. Mehrpouya, E. Graham, S.S. Park, FRF based joint dynamics modeling and identification, Mech. Syst. Signal Process. 39 (2013) 265–279.
[16] Ş. Tol, H.N. Özgüven, Dynamic characterization of bolted joints using FRF decoupling and optimization, Mech. Syst. Signal Process. 54–55 (2015) 124–138.
[17] M.L.M. Duarte, D.J. Ewins, Rotational degrees of freedom for structural coupling analysis via finite-difference technique with residual compensation, Mech. Syst. Singal Pr. 14 (2000) 205–227.
[18] Y. Champoux, V. Cotoni, B. Paillard, O. Beslin, Moment excitation of structures using two Synchronized impact hammers, J. Sound Vib. 263 (2003) 515–533.
[19] J. Tao, C.M. Mak, Error due to two-force excitation in moment mobility measurement, Appl. Acoust. 68 (2007) 1494–1501.
[20] A.S. Elliott, A.T. Moorhouse, G. Pavić, Moment excitation and the measurement of moment mobilities, J. Sound Vib. 331 (2012) 2499–2519.
[21] T.J. Gibbons, E. Öztürk, N.D. Sims, Rotational degree-of-freedom synthesis: an optimised finite difference method for non-exact data, J. Sound Vib. 412 (2018) 207–221.
[22] R. Farshidi, D. Trieu, S.S. Park, T. Freiheit, Non-contact experimental modal analysis using air excitation and a microphone array, Measurement 43 (2010) 755–765.
[23] J.R. Bell, S.J. Rothberg, Rotational vibration measurements using laser Doppler vibrometry: comprehensive theory and practical application, J. Sound Vib. 238 (2000) 673–690.
[24] S. Rothberg, J. Bell, On the application of laser vibrometry to translational and rotational vibration measurements on rotating shafts, Measurement 35 (2004) 201–210.
[25] P. Giuliani, D. DiMaio, C.W. Schwingshackl, M. Martarelli, D.J. Ewins, Six degrees of freedom measurement with continuous scanning laser Doppler vibrometer, Mech. Syst. Signal Process. 38 (2013) 367–383.
[26] M.A. Sanderson, Direct measurement of moment mobility, part II: an experimental study, J. Sound Vib. 179 (1995) 685–696.
[27] S. Jianxin, B.M. Gibbs, Measurement of point moment mobility in the presence of non-zero cross mobility, Appl. Acoust. 54 (1998) 9–26.
[28] L.H. Ivarsson, M.A. Sanderson, A.G. Troshin, Design, theory and validation of a low mass 6-d.o.f. transuducer, J. Sound Vib. 230 (2000) 661–688.
[29] L.H. Ivarsson, M.A. Sanderson, MIMO technique for simultaneous measurement of translational and rotational mobilities, Appl. Acoust. 61 (2000) 345–370.
[30] S. Jianxin, C.M. Mak, Direct measurement of moment mobility and a moment excitation system, Appl. Acoust. 63 (2002) 139–151.
[31] L.H. Ivarsson, An advanced excitation technique for measurement of unloaded multidirectional mobilities, Mech. Syst. Signal Process. 18 (2004) 1161–1186.
[32] N. Hosoya, T. Yoshimura, Estimation of frequency response function on rotational degrees of freedom of structures: cross FRFs estimation and measurement of 6-DOF FRFs, T. Jpn. Soc. Mech. Eng. C 70 (2004) 1672–1679.
[33] J.E. Mottershead, A. Kyprianou, H. Ouyang, Structural modification. Part 1: rotational receptances, J. Sound Vib. 284 (2005) 249–265.
[34] H. Xiaoyan, S.-F. Ling, A sensing and actuating transducer for measuring point impedance to moment, Measurement 43 (2010) 363–369.
[35] M. Löfdahl, R. Johnsson, A. Nykänen, Mobility measurement in six DOFs applied to the hub of a car, Appl. Acoust. 83 (2014) 108–115.
[36] N. Hosoya, I. Kajiwara, T. Hosokawa, Vibration testing based on impulse response excited by pulsed-laser ablation: measurement of frequency response function with detection-free input, J. Sound Vib. 331 (2012) 1355–1365.
[37] N. Hosoya, I. Kajiwara, K. Umenai, Dynamic characterizations of underwater structures using non-contact vibration test based on nanosecond laser ablation in water: investigation of cavitation bubbles by visualizing shockwaves using the Schlieren method, J. Vib. Control 22 (2016) 3649–3658.
[38] N. Hosoya, R. Umino, I. Kajiwara, S. Maeda, T. Onuma, A. Mihara, Damage detection in transparent materials using non-contact laser excitation by nano-second laser ablation and high-speed polarization-imaging camera, Exp. Mech. 56 (2016) 339–343.
[39] N. Hosoya, Y. Terashima, K. Umenai, S. Maeda, High spatial and temporal resolution measurement of mechanical properties in hydrogels by non-contact laser excitation, AIP Adv. 6 (2016), 095223-1–095223-8.
[40] N. Hosoya, R. Umino, A. Kanda, I. Kajiwara, A. Yoshinaga, Lamb wave generation using nanosecond laser ablation to detect damage, J. Vib. Control 24 (2018) 5842–5853.
[41] N. Hosoya, I. Kajiwara, K. Umenai, S. Maeda, Dynamic characterizations of underwater structures using noncontact vibration tests based on nano-second laser ablation in water: evaluation of passive vibration suppression with damping materials, J. Vib. Control 24 (2018) 3714–3725 .
[42] T. Yabe, C. Phipps, M. Yamaguchi, R. Nakagawa, K. Aoki, H. Mine, Y. Ogata, C. Baasandash, M. Nakagawa, E. Fujiwara, K. Yoshida, A. Nishiguchi, I. Kajiwara, Microairplane propelled by laser driven exotic target, Appl. Lett. 80 (2002) 4318–4320.
[43] Hatamleh, Effects of peening on mechanical properties in friction stir welded 2195 aluminum alloy joints, Mat. Sci. Eng. A-struct 492 (2008) 168–176.
[44] F. Huda, I. Kajiwara, N. Hosoya, Damage detection in membrane structures using non-contact laser excitation and wavelet transformation, J. Sound Vib. 333 (2014) 3609–3624.
[45] C.J. Bahr, N.S. Zawodny, B. Bertolucci, J. Li, M. Sheplak, L.N. Cattafesta, A plasma-based non-intrusive point source for acoustic beamforming applications, J. Sound Vib. 344 (2015) 59–80.
[46] J. Eskelinen, E. Hæggström, S. Delikaris-Manias, J.G. Bolaños, V. Pulkki, Beamforming with a volumetric array of massless laser spark sources – application in reflection tracking, J. Acoust. Soc. Am. 137 (2015) EL389–EL395.
[47] N. Hosoya, M. Nagata, I. Kajiwara I, R. Umino, Nano-second laser-induced plasma shock wave in air for non-contact vibration tests, Exp. Mech. 56 (2016) 1305–1311.
[48] N. Hosoya, M. Mishima, I. Kajiwara, S. Maeda, Non-destructive firmness assessment of apples using a non-contact laser excitation system based on a laser-induced plasma shock wave, Postharvest Biol. Technol. 128 (2017) 11–17.
[49] N. Hosoya, A. Yoshinaga, A. Kanda, I. Kajiwara, Non-contact and non-destructive Lamb wave generation using laser-induced plasma shock wave, Int. J. Mech. Sci. 140 (2018) 486–492.
[50] R. Akita Kajiwara, N. Hosoya, Damage detection in pipes based on acoustic excitations using laser-induced plasma, Mech. Syst. Signal Process. 111 (2018) 570–579.